Vol 11 No 7, July 2002
1009-1963/2002/11(07)/0704-06

Chinese Physics

© 2002 Chin. Phys. Soc.
and IOP Publishing Ltd

# Electron-impact ionization of $Li^+(1s^2)$ in the coplanar equal energy-sharing geometry*

Jia Xiang-Fu(贾祥富) and Liu Ming-Hai(刘明海)

*Department of Physics, Shanxi Teachers University, Linfen* 041004, *China*

(Received 30 June 2001; revised manuscript received 16 January 2002)

In this paper, the triple differential cross section for the low-energy electron impact ionization of the $Li^+$ ion is considered in the coplanar equal energy-sharing kinematics at an incident energy of 114.083 eV. The emergence of structures in the calculated cross sections is explained in terms of isolated two-body final-state interactions and three-body coupling. The cross section shows two peaks originating from 'classical' sequential two-body collisions. The position of these peaks is determined by two-body final-state interactions. In addition, it is demonstrated that the signature of three-body interactions is carried by the magnitude and ratio of these two peaks. The direct and exchange amplitudes are also considered.

**Keywords:** (e, 2e) triple differential cross sections, screening effects, Coulomb interaction, exchange effects

**PACC:** 3480D, 3450H

## 1. Introduction

Experiments for the ionization of ionic targets are limited to the total ionization and single differential cross-section measurements.[1−4] Müller *et al*[3] in their refined experiment have studied correlated two-electron transitions in the electron impact ionization of the $Li^+$ ion, and were able to observe the resonant and non-resonant double excitation leading to single ionization. They noted that the interference by resonance and direct ionization channels leads to a considerable enhancement of resonant features in the single differential and total ionization cross sections. To our knowledge, measurements of the triple differential cross section, which provides the most detailed information regarding ionization processes, have not been done until now for an ionic target.

The additional difficulty that arises in studying the electron impact ionization of an ionic target, as compared to a neutral one, is the presence of a long-range Coulomb interaction. Roy *et al*[5] in their calculation of (e, 2e) triple differential ionization cross sections for the $He^+$ ion did not include electron–electron correlation in the final channel, and as a result their final-state wavefunction dose not satisfy the proper three-body boundary conditions. Biswas and Sinha[6] suggested a model in which the scattered (faster) outgoing electron is treated in the framework of the eikonal approximation, while the ejected (slower) electron is represented by a Coulomb wave. The correlation between the two outgoing electrons is taken into account through the eikonal phase term and Coulomb parameters. Jia *et al*[7] extended the Brauner–Briggs–Klar (BBK) model[8] for hydrogen and helium ions, in which the incident electron is described by a Coulomb wave in the presence of a screened ionic nucleus and the final channel is represented by the BBK wavefunction. The basic difference between the Biswas–Sinha[6] approach and our approach[7] lies in the choice of the prescription for the final-channel wavefunction. The final-state wavefunction is chosen as the three-body Coulomb continuum (BBK),[8] which satisfies the exact three-body asymptotic boundary condition. The prescription of the latter is superior in the sense that the former is mainly appropriate for asymmetric geometric only while the latter is suitable for both the symmetric and asymmetric geometries and hence is more versatile.

The BBK model[8] should be regarded as a significant advance in the theory of (e, 2e) processes, in which a three-Coulomb (3C) product wavefunction was first used to describe the final state. This 3C wavefunction was quite successful in reproducing the

*Project supported by the Natural Science Foundation of Shanxi Province, China (Grant No 20001008) and the Science Foundation for Returnee of Shanxi Province, China (Grant No (99)13).

triple differential cross sections (TDCS) for electron impact ionization of hydrogen[8] and helium[9] at high and intermediate energies. However, for low incident energies, the calculated TDCS using the 3C wavefunction are not in agreement with experiment.[10] The major limitation of the BBK model lies in the fact that the dynamic screening of any two-body Coulomb interaction, i.e., the influence on the strength of the interaction of any two particles by the presence of a third, has not been taken into account. This deficiency was first corrected by Berakdar and Briggs[10] through the introduction of new Sommerfeld parameters for the symmetric case in which the two outgoing electrons have equal energies. Chen *et al* have extended the work of Berakdar and Briggs to both symmetric and asymmetric cases[11] and the results turned out to be in quite good agreement with the measurements.[11–15]

Therefore, in this present work we investigate mainly the ionization of $Li^+$ using the DS3C model suggested by Berakdar and Briggs.[10] The TDCS for ionization has been determined in the coplanar equal energy-sharing kinematics at an incident energy of 114.083 eV. As our aim is to explain the physical processes underlying structures observed in the TDCS, only the major features of the theory used are briefly summarized in section 2. In section 3 we concentrate on the interpretation of the angular pattern of the TDCS and in section 4 conclusions are drawn. Atomic units (a.u.) are used unless otherwise specified.

## 2. Theoretical model

The prior form of the matrix elements for the direct and exchange process of $e^- + Li^+$ ionization is given by

$$f = < \Psi_f^-(\boldsymbol{r}_1, \boldsymbol{r}_2, \boldsymbol{r}_3) \mid V_i \mid \Psi_i^+(\boldsymbol{r}_1, \boldsymbol{r}_2, \boldsymbol{r}_3) > \qquad (1)$$

and

$$g = < \Psi_f^-(\boldsymbol{r}_2, \boldsymbol{r}_1, \boldsymbol{r}_3) \mid V_i \mid \Psi_i^+(\boldsymbol{r}_1, \boldsymbol{r}_2, \boldsymbol{r}_3) > . \qquad (2)$$

The total Hamiltonian $H$ of the system is written as

$$H = H_o - \frac{(Z_t - 2)}{r_1} - \frac{Z_t}{r_2} - \frac{Z_t}{r_3} - \frac{2}{r_1} + \frac{1}{r_{12}} + \frac{1}{r_{13}} + \frac{1}{r_{23}}, \qquad (3)$$

where $Z_t$ is the charge of the helium-like target ion. The kinetic-energy operator is given by

$$H_o = -\frac{1}{2}\nabla_1^2 - \frac{1}{2}\nabla_2^2 - \frac{1}{2}\nabla_3^2, \qquad (4)$$

where $\boldsymbol{r}_1$, $\boldsymbol{r}_2$ and $\boldsymbol{r}_3$ denote the position vectors of the incoming electron '1' and the two bound electrons '2' and '3', respectively, with respect to the nucleus, and

$$\boldsymbol{r}_{12} = \boldsymbol{r}_1 - \boldsymbol{r}_2, \ \boldsymbol{r}_{23} = \boldsymbol{r}_2 - \boldsymbol{r}_3, \ \boldsymbol{r}_{13} = \boldsymbol{r}_1 - \boldsymbol{r}_3.$$

The initial channel wavefunction $\Psi_i^+$ in Eq.(1) is chosen in the framework of the Coulomb–Born approximation as

$$\Psi_i^+(\boldsymbol{r}_1, \boldsymbol{r}_2, \boldsymbol{r}_3) = F_C(\boldsymbol{k}_i, \boldsymbol{r}_1)\phi_i(\boldsymbol{r}_2, \boldsymbol{r}_3), \qquad (5)$$

where $F_C$ represents a Coulomb wavefunction due to the long-range Coulomb attraction between the incident electron and the screened target ion. This is given by

$$F_C(\boldsymbol{k}_i, \boldsymbol{r}_1) = (2\pi)^{-3/2} e^{\pi\alpha_i/2} \Gamma(1 + i\alpha_i) \times \exp[i\boldsymbol{k}_i \cdot \boldsymbol{r}_1] \, {}_1F_1[i\alpha_i; 1; i(k_i r_1 - \boldsymbol{k}_i \cdot \boldsymbol{r}_1)], \qquad (6)$$

with $\alpha_i = (z - 2)/k_i$, where $k_i$ is the initial momentum of the incident electron. The ground-state wavefunction of the helium-like ion $\phi_i(\boldsymbol{r}_2, \boldsymbol{r}_3)$ in Eq.(5) is chosen as the simple Hylleraas form

$$\phi_i(\boldsymbol{r}_2, \boldsymbol{r}_3) = u(\boldsymbol{r}_2)u(\boldsymbol{r}_3),$$

$$u(r) = \left(\frac{\lambda^3}{\pi}\right)^{1/2} e^{-\lambda r}, \qquad (7)$$

with $\lambda = (Z_t - 1) + 0.6875$. From Eqs.(3)–(6), the perturbation $V_i$ is given by

$$V_i = -\frac{(Z_t - 1)}{r_1} + \frac{1}{r_{12}} + \frac{1}{r_{13}}. \qquad (8)$$

It is evident from Eq.(8) that the perturbation $V_i$ vanishes asymptotically (for $r_1 \to \infty$, $r_2$, $r_3$ finite).

In order to construct the wavefunction $\Psi_f^-$ for the final channel, which involves four particles, we adopt the following assumptions. We have reduced the four-body problem to a three-body one in the sense that the bound passive electron plays no other role than to screen the nucleus from the two outgoing particles. For single ionization, this assumption is expected to be quite reasonable, particularly for fast electron impact.

The final-channel wavefunction $\Psi_f^-$ in Eq.(1) effectively satisfies the following equation

$$\left(H_o - \frac{Z_{sc}}{r_1} - \frac{Z_{sc}}{r_2} - \frac{Z_t}{r_3} + \frac{1}{r_{12}} - E\right)\Psi_f^- = 0, \qquad (9)$$

with the screened charge $Z_{sc} = 2$. $E$ is the total energy of system given by $E = k_1^2/2 + k_2^2/2 + \epsilon$, and $\epsilon$ is the

binding energy of the one-electron ion in its ground state. The wavefunction $\phi(r_2, r_3)$ of the two-electron ion subsystem in the final channel is represented by a symmetrized product of the one-electron ground-state wavefunction ($\phi_f$) for the bound electron ($r_3$) with the continuous wavefunction $\bar{\phi}_{k_2}$ for the ejected electron with momentum $k_2$ (orthogonalized to the ground-state orbital $u(r)$).

We write the final-channel correlated (three-body) wavefunction $\Psi_f^-$ in the following form

$$\begin{aligned}&\Psi_f^-(\boldsymbol{r}_1, \boldsymbol{r}_2, \boldsymbol{r}_3)\\ =&(2\pi)^{-3/2}\mathrm{e}^{\pi\alpha_1/2}\Gamma(1+\mathrm{i}\alpha_1)\\ &\times \exp[\mathrm{i}\boldsymbol{k}\cdot\boldsymbol{r}_1]\,{}_1F_1[-\mathrm{i}\alpha_1; 1; -\mathrm{i}(k_1 r_1 + \boldsymbol{k}_1\cdot\boldsymbol{r}_1)]\\ &\times \mathrm{e}^{\pi\alpha_{12}/2}\Gamma(1+\mathrm{i}\alpha_{12})\ {}_1F_1[-\mathrm{i}\alpha_{12}; 1;\\ &-\mathrm{i}(k_{12}r_{12} + \boldsymbol{k}_{12}\cdot\boldsymbol{r}_{12})]\phi(r_2, r_3), \end{aligned} \tag{10}$$

with

$$\phi(\boldsymbol{r}_2, \boldsymbol{r}_3) = [\bar{\phi}_{\boldsymbol{k}_2}(\boldsymbol{r}_2)\phi_f(\boldsymbol{r}_3) + \bar{\phi}_{\boldsymbol{k}_2}(\boldsymbol{r}_3)\phi_f(\boldsymbol{r}_2)]/\sqrt{2}, \tag{11}$$

$$\bar{\phi}_{k_2}(\boldsymbol{r}) = \phi_{k_2}(\boldsymbol{r}) - \langle\phi_{k_2}|u\rangle u(r). \tag{12}$$

It should be noted here that in calculating the matrix element corresponding to the second term (i.e. the exchange term) in Eq.(11), we have also replaced the coordinates '2' and '3' in the remaining part of the expression of $\Psi_f^-(\boldsymbol{r}_1, \boldsymbol{r}_2, \boldsymbol{r}_3)$ in Eq.(10) for the sake of consistency.

The ejected electron is described by the following screened Coulomb wavefunction

$$\begin{aligned}\phi_{k_2}(\boldsymbol{r}) =&(2\pi)^{-3/2}\mathrm{e}^{\pi\alpha_2/2}\Gamma(1+\mathrm{i}\alpha_2)\\ &\times \mathrm{e}^{\mathrm{i}\boldsymbol{k}_2\cdot\boldsymbol{r}_2}\ {}_1F_1[-\mathrm{i}\alpha_2; 1; -\mathrm{i}(k_2 r_2 + \boldsymbol{k}_2\cdot\boldsymbol{r}_2)]. \end{aligned} \tag{13}$$

Here, $\boldsymbol{k}_{12}$=($\boldsymbol{k}_1$–$\boldsymbol{k}_2$)/2, $k_1$ is the final momentum of the scattered electron, $\phi_f(\boldsymbol{r})$ is the ground-state wavefunction of the hydrogen-like ion, given by

$$\phi_f(r) = \left(\frac{Z_t^3}{\pi}\right)^{1/2}\mathrm{e}^{-Z_t r}, \tag{14}$$

and $\alpha_i, i \in$(1,2,12) are the Sommerfeld parameters. The assumption that the three-body system consists of three spatially-independent two-body systems leads to the representation of the Sommerfeld parameters in the BBK model[8] as $\alpha_1$=$Z_{\rm sc}/k_1$, $\alpha_2$=$Z_{\rm sc}/k_2$ and $\alpha_{12}$=$-Z_{\rm sc}/k_{12}$.

However, the Sommerfeld parameter is a measure of the strength of the Coulomb interaction between charged particles, and the strength of interaction of any two particles in the three-body Coulomb system is affected by the presence of the third. Having recognized this, Berakdar and Briggs[10] suggested the DS3C model to modify the 3C wavefunction by formulating the effective Sommerfeld parameters. Here we cite the explicit functional form for the case of equal energy sharing ($\boldsymbol{k}_1 = \boldsymbol{k}_2 = \boldsymbol{k}$) as

$$\alpha_1 = \alpha_2 = \frac{4Z_{\rm eff} - \sin\theta}{4k}, \quad \alpha_{12} = \frac{-1+\sin^2\theta}{2k\sin\theta}, \tag{15}$$

where the angle $\theta$ is defined as $\theta = (\cos^{-1}\hat{\boldsymbol{k}}_1\cdot\hat{\boldsymbol{k}}_2)/2$, and effective charge $Z_{\rm eff}$ of the $Li^{++}$(1s)-core seen by the escaping electrons is taken as[16]

$$Z_{\rm eff} = (Z_t - 1) + 0.5052\mathrm{e}^{-2.5496E}. \tag{16}$$

The electron exchange effect (between the two outgoing electrons) has been taken into account in the final channel. The exchange amplitude '$g$' can be obtained by simply interchanging $\boldsymbol{k}_1$ and $\boldsymbol{k}_2$ in the expression for the direct amplitude '$f$', i.e.,

$$g(\boldsymbol{k}_1, \boldsymbol{k}_2) = f(\boldsymbol{k}_2, \boldsymbol{k}_1).$$

Finally, the expression for the TDCS is given by (including the electron exchange effect in the final channel)

$$\mathrm{TDCS}(\boldsymbol{k}_1, \boldsymbol{k}_2) = (2\pi)^4\frac{k_1 k_2}{k_i}\left[\frac{1}{4}|f+g|^2 + \frac{3}{4}|f-g|^2\right]. \tag{17}$$

The ionization amplitude as described in Eq.(1) finally involves a three-dimensional integration, which has been evaluated numerically. For the numerical integrations we have adopted a technique similar to that of our previous work[7] with necessary modifications.

## 3. Results and discussion

We have computed the TDCS for electron impact ionization of the $Li^+$ ion at 114.083 eV incident electron energy. The coplanar equal energy-sharing geometry has been studied by taking account of electron exchange in the final channel. The results are displayed in Fig.1(a)–(d), where the present TDCS are plotted against the angle of ejection ($\theta_2$) of the ejected electron and the deflected projectile electron is detected at fixed angles of $\theta_1 = 20°, 30°, 40°, 50°$, respectively. Since no TDCS measurements have yet been performed for the ionic species, we are not in a position to compare our results with experiments.

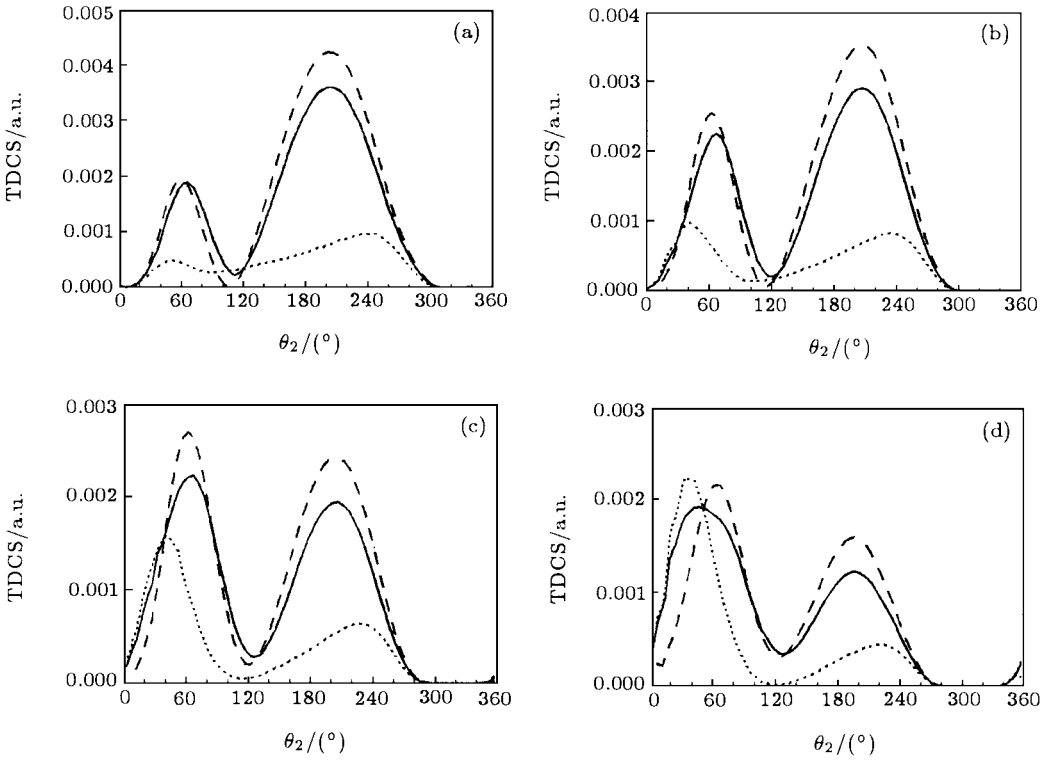



**Fig.1.** The TDCS in atomic units (a.u.) for the ionization of the $Li^+$ from the ground state (1s) by electron impact for coplanar symmetric kinematics at incident energy $E_i = 114.083\,\text{eV}$, $E_1, E_2 = 20\,\text{eV}$, as a function of ejected electron angle $\theta_2$. The scattering angle $\theta_1$ is fixed at (a) $\theta_1 = 20°$, (b) $\theta_1 = 30°$, (c) $\theta_1 = 40°$ and (d) $\theta_1 = 50°$. The solid curve represents the present results, and the dashed and dotted curves correspond to the calculations in Eqs.(1) and (2), respectively.

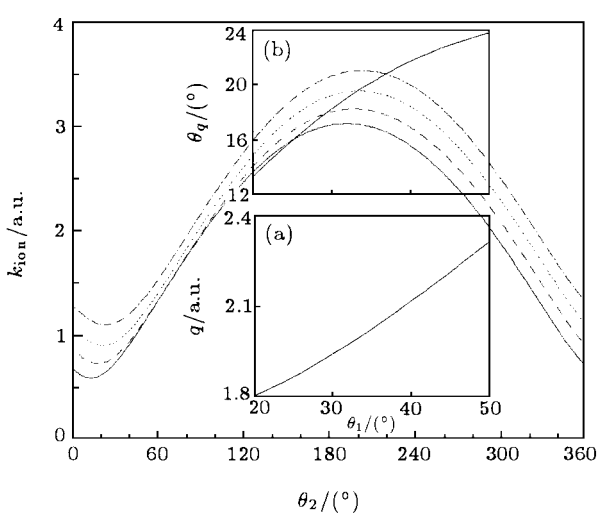



**Fig.2.** The recoil-ion momentum $k_{\text{ion}}$ as a function of the emission angle ($\theta_2$). The full, dashed, dotted and chain curves refer to the cases where $\theta_1 = 20°, 30°, 40°$ and $50°$, respectively. The inset (a) shows the behaviour of the magnitude of the momentum transfer $q$ with increasing scattering angle $\theta_1$ whereas in inset (b) the angle $\theta_q = \cos^{-1}(\hat{k}_i \cdot \hat{q})$ is depicted as a function of the scattering angle $\theta_1$ in the range investigated here.

In all cases we notice a double-peak structure in the angular distributions. Before we proceed with analysing the dynamical origin of these structures it is advantageous to study the 'classical' kinematical properties of the collisions that are common to all dynamical models. We can elucidate this by investigating the spectrum of the recoil-ion momentum. We note, as a consequence of translational invariance of the reaction, that the linear momentum is conserved during the collision, i.e. $\boldsymbol{k}_{\text{ion}}(\theta_2) = \boldsymbol{k}_i - \boldsymbol{k}_1 - \boldsymbol{k}_2$, where $\boldsymbol{k}_{\text{ion}}(\theta_2)$ is the recoil momentum of the nucleus which is assumed to be initially at rest. As seen in Fig.2, the angular behaviour of the recoil-ion momentum can be directly linked to the momentum transferred to the target during the collision, which we define as $\boldsymbol{q} = \boldsymbol{k}_i - \boldsymbol{k}_1$. If the ejected electron is emitted along $q$, the momentum transferred to the target is mainly absorbed by the secondary electron and little momentum is transferred to the nucleus (only via initial-state binding). Thus a minimum occurs in $\boldsymbol{k}_{\text{ion}}(\theta_2)$ at $\theta_2 = \theta_q = \cos^{-1}(\hat{\boldsymbol{k}}_i \cdot \hat{\boldsymbol{q}})$. This is seen nicely by comparing Fig.2 and inset (b). With increasing scattering angle $\theta_1$ of the projectile electron, the momentum transfer direction $\hat{\boldsymbol{q}}$ moves away from the incident direction (compare inset (b)

in Fig.2). The position of the minimum in $\boldsymbol{k}_{\rm ion}(\theta_2)$ exactly follows this behaviour. Besides, with increasing $\theta_1$ the magnitude of the momentum transferred to the target ion is increased as evident from inset (a) in Fig.2. Thus the overall magnitude of $\boldsymbol{k}_{\rm ion}$ is enhanced with increasing $\theta_1$. As evident from Fig.2 and inset (b), the broad peak in $\boldsymbol{k}_{\rm ion}(\theta_2)$ is located in the direction where the ionized electrons emerge opposite to the direction $\boldsymbol{q}$, i.e. at $\theta_2 = \theta_q + 180°$. The link between the structure of $\boldsymbol{k}_{\rm ion}(\theta_2)$ and $\boldsymbol{q}$ supports the identification of the minima and maxima appearing in Fig.2 as being the results of certain (sequential) two-body 'classical' collisions. In the single-binary region, where $\boldsymbol{k}_2 \| \boldsymbol{q}$, the two electrons collide almost independently of the nucleus and hence there is a minimum momentum transferred to it; the nucleus is a spectator to the electron–electron collision. Classically, the momentum transfer to the nucleus vanishes in this case provided the initial-momentum distribution of the ionic electron is neglected. The peak appearing in $\boldsymbol{k}_{\rm ion}(\theta_2)$ at the recoil region, i.e. at $(\hat{\boldsymbol{k}}_2 \cdot \hat{\boldsymbol{q}}) = -1$, can be assigned to double-binary collisions where the secondary electron scatters off the nucleus after a binary encounter with the projectile. The broadness of the peaks and minima of $\boldsymbol{k}_{\rm ion}(\theta_2)$ is due to the initial-momentum distribution of the three-body system. This broadening is more pronounced when the impact energy is lower and tends to flatten the structure in $\boldsymbol{k}_{\rm ion}(\theta_2)$. Nevertheless, it has been shown by Berakdar and Briggs,[17] that, even at excess energies as low as 2 eV, the behaviour of $\boldsymbol{k}_{\rm ion}(\theta_2)$ as described above can still be seen.

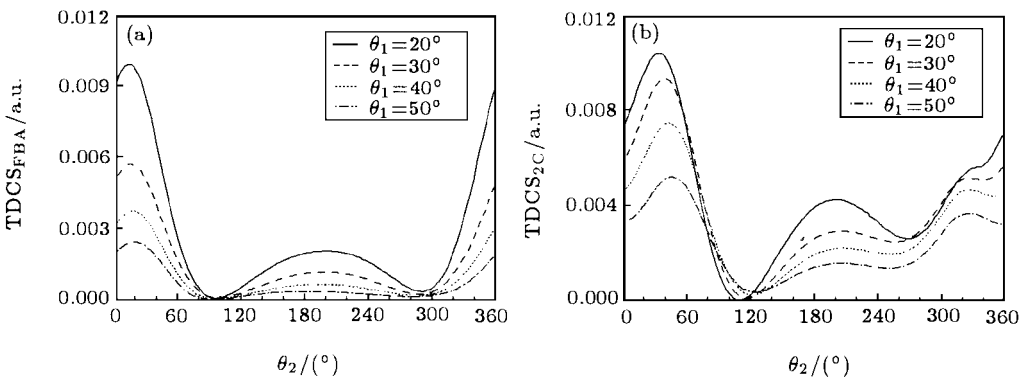



**Fig.3.** The same collision geometry as in Figs.1(a)–(d) studied in the approximations: (a) the FBA and (b) the independent Coulomb particle model (2C). The full, dashed, dotted and chain curves correspond to different fixed scattering angles, $\theta_1 = 20°, 30°, 40°$ and $50°$, respectively.

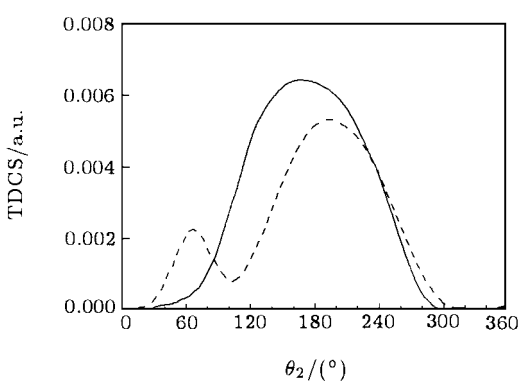



**Fig.4.** For the geometry described in Fig.1(a) the TDCS have been calculated using the projectile-ion-electron scattering amplitude ($T_{\rm ee}$ full curve), and the projectile-nucleus scattering amplitude ($T_{\rm en}$ dashed curve).

The information on $\boldsymbol{k}_{\rm ion}(\theta_2)$ can also be linked to the structure of the spin unresolved cross section, as shown in Figs.1(a)–(d). Here we observe the emergence of two peaks at positions near to the binary and recoil emission directions as discussed above. However, only the positions of these peaks can be traced to the structure of $\boldsymbol{k}_{\rm ion}(\theta_2)$ and thus to the collision-ionization mechanisms outlined above. This is evident by comparing results of different dynamical models: DS3C (Figs.1(a)–(d)), first Born approximation (FBA; in Eq.(10) $\alpha_1 = \alpha_{12} = 0$) and 2C (in Eq.(10) $\alpha_{12} = 0$; Figs.3(a) and (b)) where the kinematics are the same. The shift of the positions of these peaks is readily understood by comparing Figs.1(a)–(b) and Figs.3(a) and (b). In the FBA model, where the ionized electron occupies a target-continuum state, the position of the peaks coincides with the positions of the 'classical' binary and recoil peaks. In the 2C model, in which the two continuum electrons move independently in the nuclear field, the binary peak

is shifted away from the scattered electron direction whereas the recoil peaks appear nearer to - $\boldsymbol{k}_i$. Finally, including the electron–electron final-state interactions (Figs.1(a)–(d)) squeezes the angular distributions of the ejected electrons away from the direction of the scattering electron.

From the preceding discussion and by comparing the heights of the peaks in different dynamical models it is obvious that the magnitudes of the peaks are a subtler feature than their positions. In fact, viewed in the present theory, the actual shape of the cross section is determined by three-body coupling, as the only difference between the approximations 3C and DS3C is the inclusion of three-body coupling in the latter.[10] Three-body interactions control the interference pattern of various scattering amplitudes by differently weighting these amplitudes. This is evident from Fig.4 where the magnitudes of the scattering amplitudes from the bound electron $T_{\rm ee}$ and the nucleus $T_{\rm en}$ are examined separately. As expected, the major contribution to the cross section around the binary region comes from $T_{\rm ee}$ whereas $T_{\rm en}$ dominates over $T_{\rm ee}$ in the recoil regions. Another point which warrants investigation is the effect of the indistinguishability of the escaping electrons. The direct-scattering amplitude (see Figs.1(a)–(b)) provides the major contribution to the TDCS, i.e., the indistinguishability of the two electrons plays a minor role in determining the shape of the angular distribution.

## 4. Conclusions

The TDCS for the electron impact ionization of $Li^+$ in the coplanar equal energy sharing has been investigated at an excess energy of 40 eV. It has been shown that the cross section reveals a double-peak structure. The positions of these peaks are primarily determined by classical single- and double-binary collisions and modified by final-state interactions. It has been shown that the relative height of the peaks is the signature of three-body coupling in a three-body Coulomb system. Neglecting the coupling results in a poor description. Furthermore, it has been demonstrated that the direct ionization amplitude provides by far the major contribution to the TDCS.

## References


[1] Dolder K T and Peart B 1976 *Rep. Prog. Phys.* **39** 693
[2] Younger S M 1980 *Phys. Rev.* A **26** 3177
[3] Müller A, Hofmann G, Weissbecker B, Strenke M, Tinschert K, Wagner M and Salzborn 1989 *Phys. Rev. Lett.* **63** 758
[4] Fang D, Hu W, Tang J, Wang Y and Yang F 1993 *Phys. Rev.* A **47** 1861
[5] Roy A, Roy K and Sil N C 1982 *J. Phys. B: At. Mol. Phys.* **15** 1289
[6] Biswas R and Sinha C 1995 *J. Phys. B: At. Mol. Opt. Phys.* **28** 1311
[7] Jia X, Shi Q, Chen Z, Chen J and Xu K 1997 *Phys. Rev.* A **55** 1971
[8] Brauner M, Briggs J S and Klar H 1989 *J. Phys. B: At. Mol. Opt. Phys.* **22** 2265
[9] Brauner M, Briggs J S and Broad J T 1991 *J. Phys. B: At. Mol. Opt. Phys.* **24** 287
[10] Berakdar J and Briggs J S 1994 *Phys. Rev. Lett.* **72** 3799
[11] Chen Z, Shi Q, Zhang S, Chen J and Xu K 1997 *Phys. Rew.* A **56** R2514
[12] Chen Z, Zhang S, Shi Q, Chen J and Xu K 1997 *J. Phys. B: At. Mol. Opt. Phys.* **30** 4963
[13] Chen Z 1998 *Chin. Phys.* **7** 167
[14] Chen Z, Ni Z, Shi Q and Xu K 1998 *Chin. Phys.* **7** 481
[15] Chen Z and Xu K 2001 *Chin. Phys.* **10** 290
[16] Berakdar J and Briggs J S 1994 *J. Phys. B: At. Mol. Opt. Phys.* **27** 4271
[17] Berakdar J and Briggs J S 1996 *J. Phys. B: At. Mol. Opt. Phys.* **29** 2289